Monthly Notices
of the
ROYAL ASTRONOMICAL SOCIETY

MNRAS **458,** 3795–3807 (2016)
Advance Access publication 2016 March 11

doi:10.1093/mnras/stw582

Growth of spherical overdensities in scalar–tensor cosmologies

N. Nazari-Pooya,[1] M. Malekjani,[2⋆] F. Pace[3] and D. Mohammad-Zadeh Jassur[1]

[1]*Department of Theoretical Physics and Astrophysics, Tabriz University, Tabriz 51664, Iran*
[2]*Department of Physics, Bu-Ali Sina University, Hamedan 65178, Iran*
[3]*Jodrell Bank Centre for Astrophysics, School of Physics and Astronomy, The University of Manchester, Manchester M13 9PL, UK*

Accepted 2016 March 7. Received 2016 January 21

ABSTRACT

The accelerated expansion of the universe is a rather established fact in cosmology and many different models have been proposed as a viable explanation. Many of these models are based on the standard general relativistic framework of non-interacting fluids or more recently of coupled (interacting) dark energy models, where dark energy (the scalar field) is coupled to the dark matter component giving rise to a fifth-force. An interesting alternative is to couple the scalar field directly to the gravity sector via the Ricci scalar. These models are dubbed non-minimally coupled models and give rise to a time-dependent gravitational constant. In this work, we study few models falling into this category and describe how observables depend on the strength of the coupling. We extend recent work on the subject by taking into account also the effects of the perturbations of the scalar field and showing their relative importance on the evolution of the mass function. By working in the framework of the spherical collapse model, we show that perturbations of the scalar field have a limited impact on the growth factor (for small coupling constant) and on the mass function with respect to the case where perturbations are neglected.

Key words: cosmology: theory – dark energy – large-scale structure of Universe.

1 INTRODUCTION

Geometrical probes of the cosmic expansion scenario including: (a) Type Ia supernovae (SnIa; Riess et al. 1998; Perlmutter et al. 1999; Kowalski et al. 2008); (b) the first peak location in the angular power spectrum of cosmic microwave background (CMB) perturbations (Komatsu et al. 2009); (c) baryon acoustic oscillations in the power spectrum of the matter density field (Percival et al. 2010); (d) observations from Gamma-Ray Bursts (Basilakos & Perivolaropoulos 2008), cluster gas mass fraction (Allen et al. 2004) and the estimation of the age of Universe (Krauss & Chaboyer 2003), and dynamical probes of the growth rate of matter perturbations such as (e) the growth data from X-Ray clusters (Mantz et al. 2008); (f) the power spectrum at different redshift slices of the Ly α forest (McDonald et al. 2005; Nesseris & Perivolaropoulos 2008); (g) redshift distortions from anisotropic pattern of galactic redshifts at the cluster scales (Hawkins et al. 2003; Nesseris & Perivolaropoulos 2008) and (h) weak lensing surveys (Benjamin et al. 2007; Amendola, Kunz & Sapone 2008; Fu et al. 2008) point towards the general conclusion that our Universe is experiencing an accelerated expansion.

This cosmic expansion scenario can be well explained by assuming an additional cosmic fluid with a positive energy density and a sufficiently negative pressure usually dubbed dark energy (DE). The nature of DE is still unknown and it seems that new physics beyond the standard model of particle physics is required to explain its properties. Einstein cosmological constant Λ with constant equation of state $w_\Lambda = P_\Lambda/\rho_\Lambda = -1$ is the earliest and simplest candidate for DE. However, this model suffers from severe theoretical problems, as the fine-tuning and the cosmic coincidence problems (Weinberg 1989; Sahni & Starobinsky 2000; Carroll 2001; Padmanabhan 2003; Peebles & Ratra 2003; Copeland, Sami & Tsujikawa 2006). Alternatively, scalar fields are plausible candidates for DE (Ratra & Peebles 1988; Wetterich 1988). An outstanding feature of scalar fields is that the equation of state of these models is generally varying during the cosmic history. Moreover, due to the time varying equation of state, these models possess some fluctuations in both space and time like pressureless dust matter. Several attempts have been done to study the possibility that scalar fields might be coupled to other entities in the Universe. On one side, the coupling can be considered between scalar fields and dust matter within the framework of General Relativity (GR). On the other side, one can consider the coupling between the scalar field and the Ricci scalar, the so-called non-minimally coupled quintessence models, which is the case, for example, of scalar–tensor (ST) gravities (Bergmann 1968; Nordtvedt 1970; Wagoner 1970; Esposito-Farèse & Polarski 2001). For an historical review of ST theories see Brans & Dicke (1961) and for later attempts Perrotta, Baccigalupi & Matarrese (2000), Acquaviva, Baccigalupi & Perrotta (2004) and Pettorino & Baccigalupi (2008). Very recent

⋆ E-mail: malekjani@basu.ac.ir

parameter estimation on Brans–Dicke models have been performed by Li et al. (2015).

Beside causing the acceleration of the overall expansion rate of the Universe, quintessence models can change the formation rate and the growth of collapsed structures (haloes). It is well known that the large-scale structures we observe today originated from the small initial fluctuations originated during the inflationary phase era (Starobinsky 1980; Guth 1981; Linde 1990). These fluctuations subsequently grew under the influence of gravity (Gunn & Gott 1972; Press & Schechter 1974; White & Rees 1978; Peebles 1993; Peacock 1999; Sheth & Tormen 1999; Barkana & Loeb 2001; Peebles & Ratra 2003; Ciardi & Ferrara 2005; Bromm & Yoshida 2011).

The spherical collapse model (SCM) introduced by Gunn & Gott (1972) is a simple analytical tool to study the evolution of the growth of overdense structures on sub-horizon scales. The dynamics of the overdensities depends strongly on the dynamics of the background Hubble flow and expansion history of the Universe. In the framework of GR, the SCM has been widely investigated in the literature (Fillmore & Goldreich 1984; Bertschinger 1985; Hoffman & Shaham 1985; Ryden & Gunn 1987; Avila-Reese, Firmani & Hernández 1998; Subramanian, Cen & Ostriker 2000; Ascasibar et al. 2004; Williams, Babul & Dalcanton 2004). Furthermore, this formalism has been extended to different DE and scalar field DE cosmologies (Mota & van de Bruck 2004; Maor & Lahav 2005; Basilakos 2009; Li et al. 2009; Pace, Waizmann & Bartelmann 2010; Wintergerst et al. 2010; Basse, Eggers Bjælde & Wong 2011; Pace et al. 2012; Pace, Batista & Del Popolo 2014b; Naderi, Malekjani & Pace 2015). The growth of spherical overdensities within the framework of inhomogeneous DE cosmologies within the GR framework has been studied by Abramo et al. (2007), Abramo, Batista & Rosenfeld (2009), Pace et al. (2014b) and Malekjani, Naderi & Pace (2015).

All of the previously mentioned studies and improvements of the SCM in DE cosmologies take place within the framework of standard Einstein theory of gravity (GR). In particular, Mota & van de Bruck (2004) studied the SCM for different minimally coupled quintessence models with different potentials in the GR paradigm. However, since in ST theories there is a non-minimally coupling between the scalar field and the gravity sector via the Ricci scalar, the evolution of spherical overdensities is completely different from that of standard gravity. This is the subject of the work by Pace et al. (2014a) and Fan, Wu & Yu (2015) where the authors studied the non-linear evolution of structures in non-minimally coupled quintessence models using the SCM machinery in the context of ST gravities. It is worth to mention that in Pace et al. (2014a), despite the general derivation of the equations of motion, scalar field perturbations were assumed to be negligible to facilitate the comparison with results from *N*-body simulations. In the work by Fan et al. (2015), the non-minimally coupled quintessence models are also assumed to be homogeneous in both the metric and Palatini formalisms.

In this work, we extend the SCM in ST theory of gravity to the more general case where scalar field perturbations are taken into account. In fact in the case of GR, it was shown that density perturbations of minimally coupled scalar fields exist on all scales but they are strongly scale-dependent and negligible on sub-Hubble scales (Unnikrishnan, Jassal & Seshadri 2008; Jassal 2009, 2010). On Hubble scale, they are roughly 10 per cent of the matter density perturbations and they leave a trace on the low ℓ multipoles of the angular power spectrum of the CMB through the ISW effect (Weller & Lewis 2003). Generally, the existence of perturbations of a cosmic fluid on sub-Hubble scales depends on the effective sound speed $c_{\rm eff}$. The effective sound speed $c_{\rm eff}$ determines the sound horizon of a fluid: $l_{\rm eff} = c_{\rm eff}/H$. On scales smaller than the sound horizon, perturbations cannot grow and vanish, while on scales larger than $l_{\rm eff}$ perturbations can grow due to gravitational instability. In the case of minimally coupled quintessence models in GR, the effective sound speed is roughly equal to unity (in units of the speed of light $c = 1$). Consequently, the sound horizon is of the order of the Hubble scale H^{-1} (Ferreira & Joyce 1997, 1998; de Putter, Huterer & Linder 2010) and the perturbations of scalar fields below the horizon vanish and cannot grow. In ST gravities, the non-minimally coupling between scalar fields and curvature perturbations amplifies the scalar field perturbations on sub-Hubble scales. In addition, it has been shown that in ST theories, scalar field perturbations on sub-horizon scales are scale-independent and their effective sound speed vanishes (Esposito-Farèse & Polarski 2001). As shown by Bueno Sanchez & Perivolaropoulos (2010), scalar field perturbations are anticorrelated to the perturbations of dust matter. In addition, the ratio of the scalar field density perturbations over the matter density perturbations on sub-Hubble scales is roughly of the order of 10 per cent (Bueno Sanchez & Perivolaropoulos 2010).

The aim of this study is to generalize the SCM in ST theories of gravity for clustering non-minimally coupled quintessence models by taking the scalar field perturbations into account. We follow the evolution of perturbations both in the linear and non-linear regimes. We calculate the fundamental SCM parameters: the linear overdensity threshold $\delta_{\rm c}$ and the virial overdensity $\Delta_{\rm vir}$ in the framework of ST gravities for different homogeneous and clustering cases of non-minimally quintessence models. Having these quantity at hands, we will use them to evaluate the mass function and the number counts of haloes. We organize the paper as follows: In Section 2, we introduce the ST theories of gravity and describe the evolution of the background cosmologies in these models. In Section 3, the basic equations for the evolution of the density perturbations of the scalar field and matter are presented. In Section 4, we study the linear growth factor on sub-horizon scales and the SCM in the framework of ST gravities. We also present the effect of scalar field perturbations on the mass function and cluster number counts within the Press–Schechter formalism. Finally, we conclude and summarize our results in Section 5.

2 BACKGROUND HISTORY IN ST THEORIES

In this section, we present the background evolution equations of ST gravity in a spatially flat Friedmann–Robertson–Walker (FRW) universe. The action for these models in the physical Jordan frame is given by (Bergmann 1968; Nordtvedt 1970; Wagoner 1970)

$$S = \frac{1}{16\pi G}\int {\rm d}^4x\,\sqrt{-g}(F(\Phi)\,R - Z(\Phi)\,g^{\mu\nu}\partial_\mu\Phi\partial_\nu\Phi - 2U(\Phi)) + S_{\rm m}(g_{\mu\nu}), \quad (1)$$

where G is the gravitational coupling constant, R is the Ricci scalar, g is the determinant of the metric $g_{\mu\nu}$ and $S_{\rm m}$ is the action of the matter field which does not involve the scalar field Φ. The independence of the matter action $S_{\rm m}$ from the scalar field Φ guarantees that the weak equivalence principle is exactly satisfied. $F(\Phi)$ and $Z(\Phi)$ in equation (1) are arbitrary dimensionless functions and $U(\Phi)$ is the scalar field potential. The dynamics of the real scalar field Φ depends on the dimensionless functions $F(\Phi)$ and $Z(\Phi)$ as well as the potential $U(\Phi)$. The term $F(\Phi)R$ represents the non-minimally coupling between the scalar field Φ and gravity. In the limit of GR,

it is obvious to have $F(\Phi) = 1$, showing that there is no direct interaction between the scalar field and gravity. By a redefinition of the field Φ, the quantity $Z(\Phi)$ can be set either to 1 or -1. In this work, we will consider all equations and quantities in ST gravity for the case $Z(\Phi) = 1$. In what follows we will also use units such that $8\pi G = 1$. For a flat FRW universe with

$$\mathrm{d}s^2 = -\mathrm{d}t^2 + a^2(t)[\mathrm{d}r^2 + r^2(\mathrm{d}\theta^2 + \sin^2\theta\ \mathrm{d}\phi^2)]. \quad (2)$$

Friedmann equations for the evolution of the background in ST cosmologies are the following (see also Gannouji et al. 2006; Polarski & Gannouji 2008; Bueno Sanchez & Perivolaropoulos 2010)

$$3F(\Phi)H^2 = \rho_{\rm m} + \frac{1}{2}\dot{\Phi}^2 + U(\Phi) - 3H\dot{F}(\Phi) = \rho_{\rm tot}\ , \quad (3)$$

$$-2F(\Phi)\dot{H} = \rho_{\rm m} + \dot{\Phi}^2 + \ddot{F}(\Phi) - H\dot{F}(\Phi) = \rho_{\rm tot} + p_{\rm tot}\ . \quad (4)$$

The Klein–Gordon equation for the evolution of the scalar field and the equation of motion for non-relativistic dust matter are, respectively, given by

$$\ddot{\Phi} + 3H\dot{\Phi} = 3\frac{\mathrm{d}F}{\mathrm{d}\Phi}(\dot{H} + 2H^2) - \frac{\mathrm{d}U}{\mathrm{d}\Phi}\ . \quad (5)$$

$$\dot{\rho}_{\rm m} + 3H\rho_{\rm m} = 0\ , \quad (6)$$

where $\rho_{\rm m}$ is the energy density of pressureless dust matter. Here, we will assume the Ratra–Peebles form for the scalar field potential:

$$U(\Phi) = \frac{M^{4+\alpha}}{\Phi^{\alpha}}\ , \quad (7)$$

where M is an energy scale and the exponent α is a free positive constant. Constraints from magnitude-redshift measurements of SnIa show that $\alpha < 1$ at the $1-\sigma$ level both for minimally and non-minimally coupled quintessence models (Caresia, Matarrese & Moscardini 2004). We further assume a power law for the dimensionless function $F(\Phi)$:

$$F(\Phi) = 1 + \xi\left(\Phi^2 - \Phi_0^2\right)\ , \quad (8)$$

where the constant ξ indicates the strength of the coupling between the scalar field and Ricci scalar and Φ_0 is the value of the scalar field at the present time (see also Perrotta et al. 2000; Perrotta & Baccigalupi 2002). Solar system tests put very tight constraints on the coupling parameter $\xi \approx 10^{-2}$, (see Reasenberg et al. 1979; Chiba 1999; Uzan 1999; Riazuelo & Uzan 2002; Bertotti, Iess & Tortora 2003).

From equations (3) and (4), the energy density and pressure of the scalar field in the framework of ST gravities (in the case of $Z(\Phi) = 1$ assumed here) can be easily obtained as follows:

$$\rho_\phi = \frac{1}{2}\dot{\Phi}^2 + U(\Phi) - 3H\dot{F}(\Phi)\ , \quad (9)$$

$$p_\phi = \frac{1}{2}\dot{\Phi}^2 - U(\Phi) + \ddot{F}(\Phi) + 2H\dot{F}(\Phi)\ . \quad (10)$$

We now solve numerically the coupled system of equations (3, 4, 5 and 6) for the above potentials $U(\Phi)$ and $F(\Phi)$. We fix the initial time at matter-radiation equality epoch $a_{\rm i} \approx 10^{-4}$ and also set the present time values of the scalar field and energy density of pressureless dust matter as $\Phi_0 = 1$ and $\Omega_{\rm m,0} = 0.30$, respectively. We also need two initial conditions to solve the Klein–Gordon equation. Following Bueno Sanchez & Perivolaropoulos (2010), we set the initial conditions as $\Phi(a_{\rm i}) = 0.12$ and $\dot{\Phi}(a_{\rm i}) = 10^{-5}$. We have two free parameters, ξ and α, in this analysis. It should be emphasized that the initial values of these parameters must be chosen such that the function $F(\Phi)$ and the scalar field Φ evolve from their initial values to reach $F(\Phi) = 1$ and $\Phi = \Phi_0 = 1$ at the present time. Consequently, the amount of energy density of the scalar field Ω_Φ should be close to 0.70 at the present time. On the basis of different values of the exponent parameter of the scalar field potential, α, and the strength of the non-minimally coupling, ξ, we adopt four different cosmological models in the framework of ST gravities presented in Table 1. The concordance Λ cold dark matter (ΛCDM) model is reproduced by setting $\alpha = 0$ and $\xi = 0$. Also model (3) represents a minimally coupled quintessence model in which there is no direct coupling between the scalar field and gravity ($\xi = 0$).

Table 1. Different minimally and non-minimally coupled quintessence models considered in this work. The parameter α indicates the exponent of the inverse power-law potential and ξ represents the strength of the coupling between the scalar field and gravity.

Model	ξ	α
Model (1)	0.123	0.261
Model (2)	0.088	0.679
Model (3)	0.000	0.877
Model (4)	−0.087	0.877
ΛCDM	0.000	0.000

In Fig. 1, we show the evolution of $1/F(\Phi)$ (top panel), $U(\Phi)$ (middle panel) and Φ (bottom panel), as a function of redshift z for the different cosmological models presented in Table 1. Line styles and colours for each model have been indicated in the caption. While $1/F(\Phi)$ is almost constant at high redshifts and its variation with cosmic z is very small, it changes rapidly at low redshifts and reaches one at present time. The constant line $1/F(\Phi) = 1$ represents model (3), the minimally coupled quintessence model with $\xi = 0$, as expected. In the next section, we will see that the effective gravitational constant in ST cosmologies is proportional to $1/F(\Phi)$. In middle panel of Fig. 1, we show the evolution of the Ratra–Peebles potential for the different models of Table 1. In all the models, the potential decays from larger values at higher redshift to one at the present time. In fact we fix the potential to be one at the present time by setting $\Phi_0 = 1$ and $M = 1$. We see that for the non-minimally coupled cases, independently of the sign of ξ, the potential is weaker compared to the minimally coupled case in GR. A larger value of the coupling parameter ξ causes stronger deviations from the potential in GR gravity. Finally, in the bottom panel, we present the redshift evolution of the scalar field Φ for different models. We see that for all models the scalar field increases with redshift from its small initial value at $a_i = 10^{-4}$ to $\Phi_0 = 1$ at the present time.

We now calculate the redshift evolution of the background cosmological parameters: the equation of state of the scalar field, $w_\Phi = p_\Phi/\rho_\Phi$, the energy density parameter of the scalar field, Ω_Φ and the Hubble expansion rate H, for the different cosmological models considered in this work. As well known, these quantities can describe the background evolution of the universe. Moreover, the linear growth rate of structures strongly depends on the background evolution. In Fig. 2, using equations (9) and (10), we first show the evolution of w_Φ as a function of the redshift z (top panel). We then show the redshift evolution of the energy density Ω_Φ for our selected models and Ω_Λ for concordance ΛCDM model (middle panel). We finally present the evolution of the fractional difference of the Hubble parameter $\Delta H(z)$ for these models relatively to the

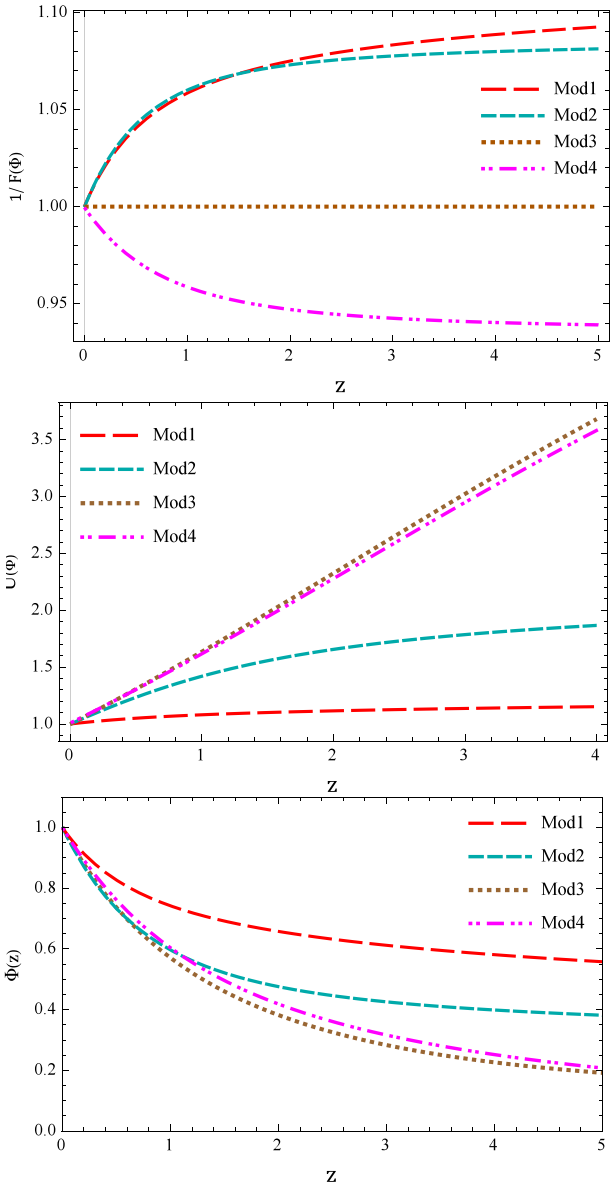

Figure 1. The redshift evolution of $1/F(\Phi)$ (top panel), the Ratra–Peebles potential $U(\Phi)$ (middle panel) and the scalar field (bottom panel) for the different cosmological models in ST cosmologies considered in Table 1. The pink dot–dotted–dashed curve stands for the negative coupling constant, ($\xi < 0$, model 4). The red long-dashed curve indicates the positive coupling $\xi = 0.123$ (model 1), the green short-dashed curve corresponds to the positive coupling $\xi = 0.088$ (model 2) and the brown dotted line represents the minimally coupled model $\xi = 0$ (model 3).

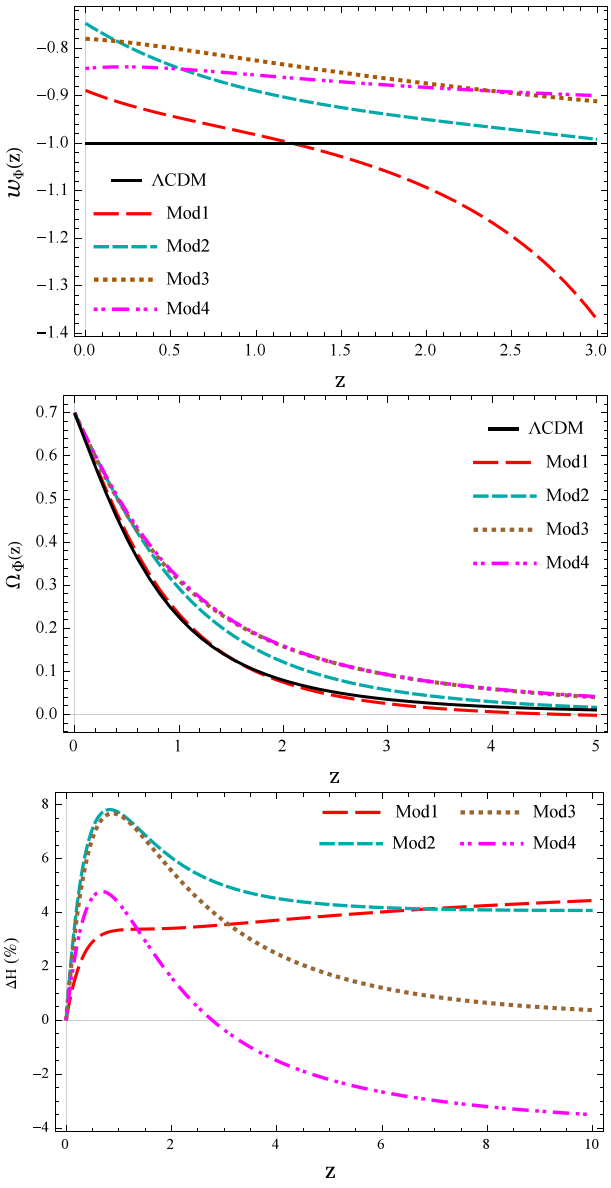

Figure 2. Top panel: the redshift evolution of the equation of state w_Φ. Middle panel: the energy density of the minimally and non-minimally coupled quintessence models (Ω_Φ) and Ω_Λ for the reference ΛCDM model (black solid curve). Bottom panel: the relative difference of the Hubble parameter in the framework of different minimally and non-minimally coupled quintessence models ($\Delta H(z)$) relative to the one of the reference ΛCDM model $H_{\Lambda\mathrm{CDM}}$. Line styles and colours are the same as in Fig. 1.

concordance ΛCDM model $H_{\Lambda\mathrm{CDM}}(z)$ in the bottom panel of Fig. 2. We refer to the caption for the different colours and line styles. In the case of a positive coupling ($\xi > 0$), the phantom regime ($w < -1$) can be achieved at high redshifts, while models with $\xi < 0$ and $\xi = 0$ remain in the quintessence regime ($w > -1$). The amount of DE for different minimally and non-minimally coupled quintessence models as well as the ΛCDM model have been presented in the middle panel. For all the models the amount of DE is negligible at high redshifts meaning that all the models reduce to an Einstein de Sitter (EdS) Universe at early times. The evolution of $\Delta H(z)$ for different models is shown in the bottom panel. As it appears clear, at low redshifts, all the models give $\Delta H(z) > 0$ indicating that all of them have larger Hubble parameter than the ΛCDM universe. We see that at high redshifts the Hubble parameter becomes smaller than the reference one only for a negative coupling constant (model 4). In the case of the minimally coupled quintessence (model 3), the Hubble parameter tends to the fiducial value in the ΛCDM model at high redshifts and differences become negligible. This result is interesting, because in this model there is no direct coupling between the scalar field and gravity and therefore DE models mimics the cosmological constant at high redshifts. In the case of non-minimally coupled quintessence models with positive coupling $\xi > 0$ (models 1 and 2), differences with respect to the ΛCDM model are at most 4 per cent at high redshifts for both

models, independently of the exact value of ξ. We conclude that in ST theories of gravity, the coupling between the scalar field and the gravitational sector causes differences in the Hubble expansion rate with respect to the ΛCDM universe also at high redshifts. More in detail, at high redshifts differences are positive (negative) for positive (negative) values of the coupling constant ξ. In the next section, we will see that differences of the Hubble parameter together with the time evolution of the gravitational constant lead to differences in the growth of matter perturbations in ST theories with respect to the standard general relativistic models.

3 PERTURBATIONS IN ST GRAVITIES

Let us start with the perturbed FRW metric in the Newtonian gauge (Boisseau et al. 2000; Esposito-Farèse & Polarski 2001; Bueno Sanchez & Perivolaropoulos 2010)

$$\mathrm{d}s^2 = -(1+2\phi)\mathrm{d}t^2 + a^2(1-2\psi)\delta_{ij}\,\mathrm{d}x^i\,\mathrm{d}x^j\ , \tag{11}$$

where ϕ and ψ are the linear gravitational potentials. In the framework of GR and in the absence of anisotropic stresses, it is obvious to have $\phi = \psi$. In ST theories of gravity, this is no longer true and the two potentials can be related to each other as (Boisseau et al. 2000; Esposito-Farèse & Polarski 2001; Bueno Sanchez & Perivolaropoulos 2010):

$$\phi = \psi - \frac{F_{,\Phi}}{F}\delta\Phi\ , \tag{12}$$

where $F_{,\Phi} = \mathrm{d}F/\mathrm{d}\Phi$. For $F = 1$ (as in GR gravity), equation (12) gives $\phi = \psi$ as expected. The general relativistic equations for the perturbations of ϕ, ψ and the scalar field Φ in ST theories of gravity have been studied in details by Esposito-Farèse & Polarski (2001), Hwang & Noh (2005), Copeland et al. (2006) and Bueno Sanchez & Perivolaropoulos (2010).

The linear evolution of non-relativistic matter density perturbations and scalar field perturbations in the framework of ST theory of gravity can be written as follows (Copeland et al. 2006; Bueno Sanchez & Perivolaropoulos 2010):

$$\ddot{\delta}_\mathrm{m} + 2H\dot{\delta}_\mathrm{m} + \frac{k^2}{a^2}\left(\psi - \frac{F_{,\Phi}}{F}\delta\Phi\right) - 3(\ddot{\psi} + 2H\dot{\psi}) = 0\ , \tag{13}$$

where k is the wavenumber of the perturbations mode. Since in this work we deal with the SCM formalism with perturbations well inside the horizon scale, in the following we will limit ourselves to the study of perturbations of matter and scalar fields on scales much smaller than the Hubble scale ($k/a \gg H$). On these scales, the scalar field perturbations can be obtained as (Bueno Sanchez & Perivolaropoulos 2010):

$$\delta\Phi \simeq (\phi - 2\psi)F_{,\Phi}\ . \tag{14}$$

Using equation (12), we have

$$\delta\Phi \simeq -\psi\,\frac{F F_{,\Phi}}{F + F_{,\Phi}^2}\ , \tag{15}$$

showing that the perturbations of non-minimally coupled scalar fields in ST gravity are scale independent on sub-horizon scales. For minimally coupled scalar field models in GR, since $F = 1$ and consequently $F_{,\Phi} = 0$, it is trivial to see that $\delta\Phi = 0$. Hence scalar field perturbations on sub-horizon scales are negligible for minimally coupled quintessence models in GR gravity (see also Unnikrishnan et al. 2008; Jassal 2009, 2010, 2012; Bueno Sanchez & Perivolaropoulos 2010).

It has been shown that on sub-horizon scales, the energy density perturbation of the non-minimally coupled DE, $\delta\rho_\Phi$, can be expressed as a function of scalar field perturbation $\delta\Phi$ as follows (Bueno Sanchez & Perivolaropoulos 2010):

$$\delta\rho_\Phi \simeq -\frac{k^2}{a^2}F_{,\Phi}\delta\Phi = \frac{k^2}{a^2}\psi\,\frac{F\,F_{,\Phi}^2}{F + F_{,\Phi}^2}\ . \tag{16}$$

Also, matter density perturbations are (Bueno Sanchez & Perivolaropoulos 2010):

$$\delta\rho_\mathrm{m} \simeq -\frac{k^2}{a^2}\psi F\left(\frac{F_{,\Phi}^2}{F + F_{,\Phi}^2} + 2\right)\ . \tag{17}$$

Hence, the ratio $\frac{\delta\rho_\Phi}{\delta\rho_m}$ on sub-horizon scales is given by

$$\frac{\delta\rho_\Phi}{\delta\rho_\mathrm{m}} = \frac{\delta_\Phi}{\delta_\mathrm{m}} \simeq -\frac{F_{,\Phi}^2}{3F_{,\Phi}^2 + 2F}\ . \tag{18}$$

Using equations (16) and (18), we can eliminate the term $\frac{k^2}{a^2}\psi$ from equation (13) and being the study of the perturbations limited to the sub-horizon scales, we can also ignore the time derivatives of the potential ψ in equation (13) (see also Boisseau et al. 2000; Bueno Sanchez & Perivolaropoulos 2010). In this case, it is easy to obtain the linear evolution of matter overdensities on sub-horizon scales within ST gravities as (see also Boisseau et al. 2000)

$$\ddot{\delta}_\mathrm{m} + 2H\dot{\delta}_\mathrm{m} - 4\pi G_\mathrm{eff}\rho_\mathrm{m}\delta_\mathrm{m} = 0\ , \tag{19}$$

where the effective gravitational constant G_eff reads:

$$G_\mathrm{eff}^{(p)} = \frac{G_\mathrm{N}}{F}\left(\frac{2F + 4F_{,\Phi}^2}{2F + 3F_{,\Phi}^2}\right)\ , \tag{20}$$

where (p) represents the clustering non-minimally coupled quintessence models. We see that equation (19) is scale independent (as in the GR case) but the Newtonian gravitational constant G_N is replaced by the effective gravitational constant G_eff as given by equation (20). In fact, the effect of scalar field perturbations $\delta\Phi$ is included in the definition of G_eff. In the case of homogeneous non-minimally coupled models where we ignore the perturbations of scalar field ($\delta\Phi = 0$), it is easy to show that:

$$\frac{k^2}{a^2}\psi = -4\pi\rho_\mathrm{m}\delta_\mathrm{m}\frac{1}{F}\left(\frac{2F + 2F_{,\Phi}^2}{2F + 3F_{,\Phi}^2}\right)\ . \tag{21}$$

Inserting equation (21) into equation (13) and ignoring the time derivatives of ψ in the sub-Hubble scale regimes, we again obtain equation (19) for the evolution of matter overdensity in homogeneous non-minimally quintessence models with $\delta\Phi = 0$, but in this case the effective gravitational constant G_eff is reduced to (see also Pace et al. 2014a):

$$G_\mathrm{eff}^{(h)} = \frac{G_\mathrm{N}}{F}\left(\frac{2F + 2F_{,\Phi}^2}{2F + 3F_{,\Phi}^2}\right)\ , \tag{22}$$

where (h) indicates the homogeneous scenarios. In Fig. 3, we show the redshift variation of the difference between $G_\mathrm{eff}^{(p)}$ and $G_\mathrm{eff}^{(h)}$ divided by the Newtonian gravitational constant G_N, $\Delta G_\mathrm{eff}/G_\mathrm{N} = (G_\mathrm{eff}^{(p)} - G_\mathrm{eff}^{(h)})/G_\mathrm{N}$, where $G_\mathrm{eff}^{(p)}$ is the effective gravitational constant for clustering non-minimally coupled models and $G_\mathrm{eff}^{(h)}$ is for the homogeneous case, respectively, defined in equations (20 and 22). In the case of model (3), we see that the relative difference $\Delta G_\mathrm{eff}/G_\mathrm{N} = 0$. This result is expected, since there are no perturbations of scalar field in this model and the effective gravitational constant is given by equation (22). In the case of models (1, 2 and 4),

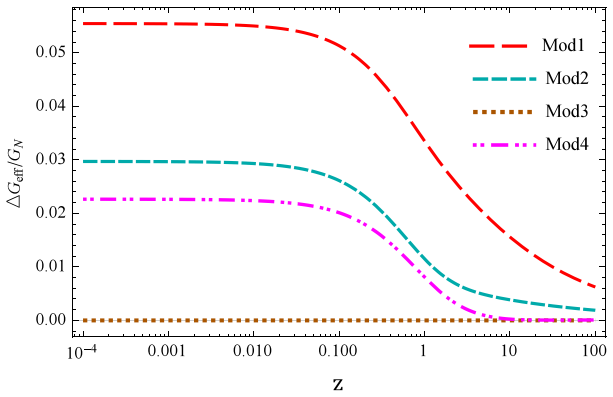

Figure 3. The redshift variation of the difference between the effective gravitational constant defined in clustering non-minimally coupled quintessence models $G_{\rm eff}^{(p)}$ and the same quantity in homogeneous non-minimally coupled quintessence models $G_{\rm eff}^{(h)}$, divided by Newtonian gravitational constant $G_{\rm N}$ as $\Delta G_{\rm eff}/G_{\rm N} = (G_{\rm eff}^{(p)} - G_{\rm eff}^{(h)})/G_{\rm N}$. Line styles and colours are the same as in Fig. 1.

the non-minimally coupled models, we see that $\Delta G_{\rm eff}/G_{\rm N} > 0$ at low redshifts and approaches zero at high redshifts. Since the difference between $G_{\rm eff}^{(p)}$ and $G_{\rm eff}^{(h)}$ at high redshifts is zero, we conclude that the perturbations of the scalar field, which directly influence the effective gravitational constant, can be neglected at early times. On the other hand, at low redshifts, since $\Delta G_{\rm eff} > 0$, we can say that the effective gravitational constant defined in clustering non-minimally quintessence models, $G_{\rm eff}^{(p)}$, is bigger than the corresponding quantity defined in homogeneous non-minimally quintessence models. Moreover in model (1), where the strength of non-minimally coupling between scalar field and gravity is the largest, the difference between $G_{\rm eff}^{(p)}$ and $G_{\rm eff}^{(h)}$ is the largest (roughly 5.5 per cent) among the other models. On the basis of the above discussion, it is easy to see that due to the different behaviours of the definition of the effective gravitational constant $G_{\rm eff}$ in clustering and homogeneous versions of non-minimally coupled models, matter overdensity will evolve differently whether the scalar field perturbations are taken into account or not. In the next section, we solve equation (19) in order to follow the evolution of matter overdensities on sub-Hubble scales in the linear regime for these two different classes of models. We also compare these models with the minimally coupled quintessence model in GR gravity.

4 GROWTH OF OVERDENSITIES IN ST GRAVITIES

In this section, we study the growth of structures on sub-horizon scales in the framework of ST gravity for different homogeneous and clustering models. In particular, we evaluate the linear evolution of perturbations and the growth factor in Section 4.1, the non-linear evolution and the spherical collapse parameters in Section 4.2 and the mass function for virialized haloes in Section 4.3.

4.1 Growth factor

Here we follow the linear growth of perturbations of non-relativistic dust matter and density perturbations of the scalar field by solving equations (18) and (19). We remind the reader that in the case of clustering quintessence models where the effects of scalar field perturbations are taking into account, the effective gravitational

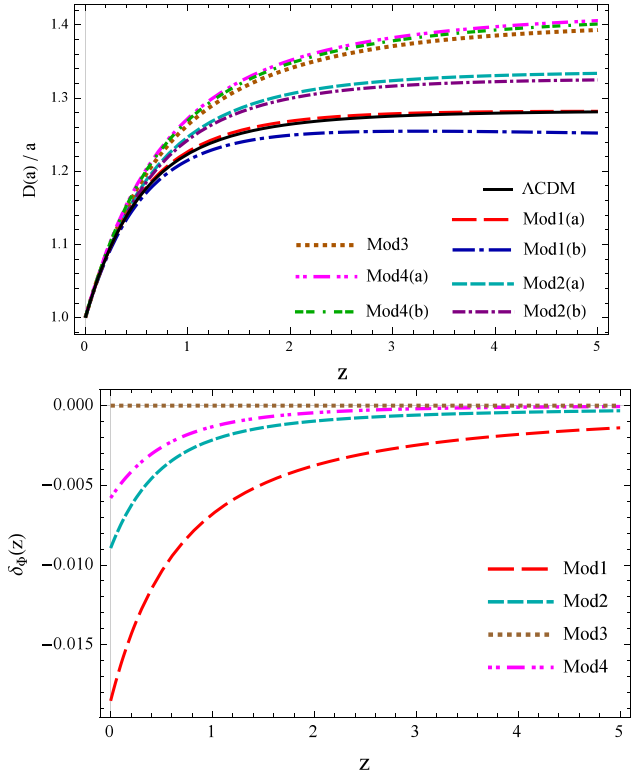

Figure 4. Top panel: redshift evolution of the growth factor normalized to one at the present time divided by the scale factor a in terms of the cosmic redshift z for different cosmological models considered in Table 1. For all the models, label (a) represents homogeneous models and label (b) indicates the clustering cases. The red long dashed (blue dotted–long-dashed) curve represents homogeneous (clustering) models with coupling parameter $\xi = 0.123$ (model 1). The cyan dashed (violet dot–dashed) curve represents the homogeneous (clustering) model with $\xi = 0.088$ (model 2). The brown dotted curve indicates the minimally coupled quintessence model with $\xi = 0.00$ (model 3). The pink double dot–dashed (green double dash–dot) curve represents the homogeneous (clustering) model with $\xi = -0.087$ (model 4). The reference ΛCDM model is shown by a black solid curve for comparison. Bottom panel: evolution of the density perturbations of the scalar field δ_Φ according to equation (18). Line styles and colours are as in Fig. 1.

constant $G_{\rm eff}$ is given by equation (20), while in the case of homogeneous models, we adopt equation (22). It is also obvious, in the case of minimally coupled quintessence models ($\xi = 0$), that we have $G_{\rm eff} = G_{\rm N}$ as expected.

In Fig. 4, we show the linear growth factor $D_+(a) = \delta_{\rm m}(a)/\delta_{\rm m}(a = 1)$ divided by the scale factor $(D_+(a)/a)$ as a function of redshift z for the different cosmological models studied in this work (top panel). In the bottom panel, we show the evolution of the density perturbations of DE δ_Φ in terms of the redshift z. In all cases, label (a) represents homogeneous models and label (b) indicates the clustering case. Line style and colours have been described in the caption of the figure. While model (3), the minimally coupled case, has a larger growth factor compared to the reference ΛCDM universe at high redshifts, we see that the non-minimally coupled models with negative (positive) coupling constant ξ have a higher (lower) growth factor with respect to the minimally coupled model. For all the models, the decrease of the growth factor at lower redshifts is due to the fact that at late times DE dominates the energy budget of the universe and suppresses the amplitude of perturbations. Also, the constant behaviour at high redshifts shows that at early times the

effects of DE are negligible for all the models. In the non-minimally coupled cases, we conclude that the growth factor is smaller for clustering models compared to the homogeneous case. The difference between the growth factor of clustering and homogeneous models is more pronounced for higher values of the coupling constant ξ. In fact the decrease of the growth factor in clustering DE models compared to the homogeneous models is due to the fact that the density perturbation of the DE field is always negative ($\delta_\Phi < 0$) as shown in the bottom panel of Fig. 4. In addition, the negative value of δ_Φ is due to the minus sign in equation (18) and one can see that clustering DE models can reproduce void DE structures (see also Dutta & Maor 2007; Unnikrishnan et al. 2008; Jassal 2009, 2012; Mainini 2009; Bueno Sanchez & Perivolaropoulos 2010; Villata 2012).

4.2 SCM parameters

The linear overdensity parameter δ_c and the virial overdensity Δ_{vir} are the two main quantities characterizing the SCM. In this section, we evaluate them in the framework of ST cosmologies.

The linear overdensity δ_c is an important quantity in the Press–Schechter formalism (Press & Schechter 1974; Bond et al. 1991; Sheth & Tormen 2002) and the virial overdensity Δ_{vir} is used to determine the size of virialized haloes.

To derive the time evolution of the linear overdensity parameter δ_c, we use the following non-linear evolution equation (Pace et al. 2014a)

$$\ddot{\delta}_m + 2H\dot{\delta}_m - \frac{4}{3}\frac{\dot{\delta}_m^2}{1+\delta_m} - 4\pi G_{eff}\rho_m\delta_m = 0\,, \qquad (23)$$

where in the case of homogeneous models G_{eff} is given by equation (22) and in the case of clustering models we use equation (20). Remember that in the case of the minimally coupled model (model 3 in our analysis), the effective gravitational constant G_{eff} reduces to the constant Newtonian gravitational constant G_N in the GR limit. It is important to note that the evolution of matter perturbations in ST cosmologies both in the linear (equation 19) and non-linear (equation 23) regime are coupled to the perturbations of the scalar field δ_Φ through the effective gravitational constant G_{eff} introduced in equations (20) for clustering non-minimally coupled DE models. We should emphasize that although the functional form of equations (19 and 23) for the evolution of matter perturbations is identical to that obtained in standard GR once G_N is replaced by G_{eff}, differences between the two gravitational models are deeper. In fact G_{eff} in ST theory is dynamical and evolves in time, while G_N is constant in GR. Moreover, the perturbations of the scalar field δ_Φ affect directly the evolution of G_{eff} via equation (20). This feature of ST theory completely determine the behaviour of the growth of matter perturbations in ST cosmologies with respect to the standard perturbations growth in GR models. Said this, we follow the general approach outlined in Pace et al. (2010, 2012, 2014a) to determine the linear overdensity δ_c and virial overdensity Δ_{vir}, to which we refer for an in depth description of the procedure.

In Fig. 5, we show the evolution of δ_c as a function of the collapse redshift z_c for the models presented in Table 1. We refer to the caption for line styles and colours. In analogy to the previous section, label (a) represents homogeneous models and label (b) indicates clustering models. We see that at low redshifts, where DE dominates the energy budget of the Universe, δ_c for clustering models is smaller than that obtained in the homogeneous case. In fact the perturbations of the scalar field due to the non-minimally coupling between the scalar field and the Ricci scalar lowers the value of δ_c

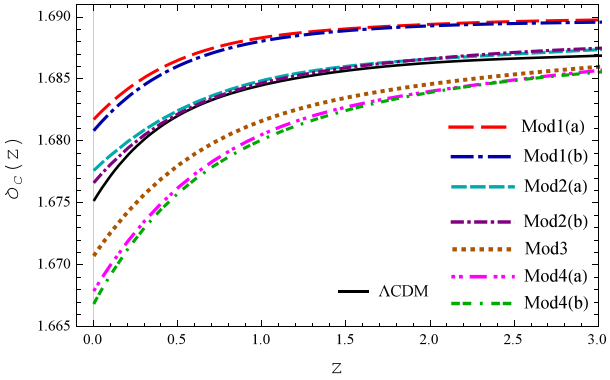

Figure 5. Linear overdensity parameter δ_c as a function of the collapse redshift z_c for different minimally and non-minimally coupled models considered in this work. Line styles and colours are as in Fig. 4.

at low redshifts. This results is expected, since we showed that the density perturbations of scalar fields due to the non-minimally coupling are always negative (see bottom panel of Fig. 4). Furthermore, one can see that for positive (negative) coupling constant ξ the value of δ_c is larger (smaller) compared to the minimally coupled model (e.g. model 3).

In addition to δ_c, the other important parameter in the SCM is the virial overdensity Δ_{vir}. The size of spherically symmetric haloes can be well defined by the virial overdensity parameter. The virial overdensity is defined as $\Delta_{vir} = \zeta(x/y)^3$, where ζ is the overdensity at the turn-around redshift, x is the scale factor normalized to the turn-around scale factor and y is the ratio between the virialized radius and the turn-around radius (Wang & Steinhardt 1998). In EdS cosmology, it is well known that $y = 1/2$, $\zeta \approx 5.6$ and $\Delta_{vir} \approx 178$ at any cosmic redshift. In DE cosmologies, Δ_{vir} depends on the evolution of the DE sector and evolves with redshift. Moreover, according to whether DE takes part or not into the virialization process, the quantity y may be larger or smaller than $1/2$. Hence the virial overdensity Δ_{vir} can be affected by the clustering of DE (Maor & Lahav 2005; Pace et al. 2014b; Malekjani et al. 2015).

In standard cosmology, the virialization of pressureless dust matter and size of forming haloes are strongly affected by the DE component (Lahav et al. 1991; Wang & Steinhardt 1998; Mota & van de Bruck 2004; Horellou & Berge 2005; Wang & Tegmark 2005; Naderi et al. 2015) and also by DE perturbations (Abramo et al. 2007, 2008, 2009; Batista & Pace 2013; Pace et al. 2014b; Malekjani et al. 2015). In ST cosmologies, we expect that the density perturbations of the scalar field derived from the non-minimally coupling between the scalar field and Ricci scalar affect the evolution of the virial overdensity Δ_{vir}.

In Fig. 6, we show the redshift evolution of the virial overdensity Δ_{vir} for different homogeneous (top panel) and clustering (bottom panel) models in ST theory. All clustering and homogeneous quintessence models reach the fiducial value $\Delta_{vir} \approx 178$ at high redshifts and decrease towards smaller redshift values. This result is expected, since at high redshifts the effect of DE on the scenario of structure formation is negligible and the EdS cosmology is recovered. A decrease in Δ_{vir} with redshift z in ST cosmologies indicates that the quintessence sector in ST gravity prevents collapse and condensation of overdense regions as it happens for DE models in standard GR gravity. For $a \approx 1$ the difference between clustering and homogeneous quintessence models is limited. We see that in homogeneous models the virial overdensity is slightly bigger than in the clustering case. Quantitatively speaking, the present value

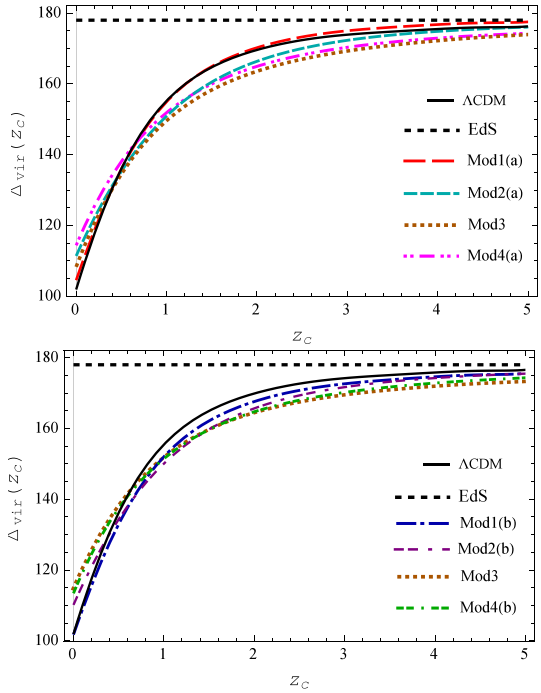

Figure 6. Virial overdensity parameter $\Delta_{\rm vir}$ as a function of collapse redshift z for different models given in Table 1. The top panel shows non-clustering models while the bottom panel represents the clustering case. Line styles and colours are as in Fig. 4.

of $\Delta_{\rm vir}$ in model (1a) is roughly 3 per cent larger than model (1b). In the case of homogeneous models (2a) and (4a), $\Delta_{\rm vir}$ is almost 1 per cent higher than clustering cases (2b) and (4b).

4.3 Abundance of haloes in homogeneous quintessence models

We now estimate the comoving number density of virialized haloes in a certain mass range. To this end, we adopt the Press–Schechter formalism in which the abundance of haloes is described in terms of their mass (Press & Schechter 1974). In the Press–Schechter formalism, the fraction of the volume of the Universe which collapses into an halo of mass M at a given redshift z is expressed by a Gaussian distribution function (Press & Schechter 1974; Bond et al. 1991). The comoving number density of haloes with masses in the range of M and $M + {\rm d}M$ as a function of the redshift z is given by

$$\frac{{\rm d}n(M, w, z)}{{\rm d}M} = \frac{\bar{\rho}_0}{M}\frac{{\rm d}\nu(M, w, z)}{{\rm d}M} f(\nu) \,, \tag{24}$$

where $\bar{\rho}_0$ is the background density at the present time and

$$\nu(M, w, z) = \frac{\delta_{\rm c}}{\sigma} \,, \tag{25}$$

where σ is the r.m.s. of the mass fluctuations in spheres containing the mass M. Generally, the parameters $\delta_{\rm c}$ and σ depend on the cosmological model and as a consequence also on the equation of state of the DE component. Although, the standard mass function $f(\nu)$ presented in Press & Schechter (1974) can provide a good estimate of the predicted number density of haloes, it fails by predicting too many low-mass haloes and too few high-mass objects (Sheth & Tormen 1999, 2002). Hence we use a modified mass function proposed by Sheth & Tormen (1999, 2002):

$$f(\nu) = 0.2709\sqrt{\frac{2}{\pi}}\left(1 + 1.1096\nu^{0.3}\right)\exp\left(-\frac{0.707\nu^2}{2}\right) . \tag{26}$$

Adopting a Gaussian density field, the amplitude of mass fluctuation $\sigma(M)$ is given by

$$\sigma^2 = \frac{1}{2\pi^2}\int_0^\infty k^2 P(k) W^2(kR){\rm d}k \,, \tag{27}$$

where R is the radius of the overdense spherical region, $W(kR)$ is the Fourier transform of a spherical top-hat filter and $P(k)$ is the linear power spectrum of density fluctuations (Peebles 1993). The number density of virialized haloes above a certain mass M at collapse redshift z is

$$n(>M, z) = \int_M^\infty \frac{{\rm d}n(z)}{{\rm d}M'}{\rm d}M' \,. \tag{28}$$

We now compute the predicted number density of virialized haloes in the Press–Schechter formalism for homogeneous models in ST cosmologies. In the case of homogeneous cosmologies we use equations (24) and (28) to determine the number density of virialized haloes. In this case the total mass of haloes is defined by the pressureless matter perturbations. In order to calculate σ^2, we adopt the formulation presented in Abramo et al. (2007) and Naderi et al. (2015). On the basis of latest observational results by the Planck Collaboration team (Planck Collaboration XIII 2015), we adopt the concordance ΛCDM model with the normalization of the matter power spectrum $\sigma_8 = 0.815$.

In Fig. 7, we show the ratio of the predicted number of haloes above a given mass M between the homogeneous models in ST gravity and the concordance ΛCDM universe for different cosmic redshifts: $z = 0$ (top-left panel), $z = 0.5$ (top-right panel), $z = 1.0$ (bottom-left panel) and $z = 2.0$ (bottom-right panel). Analogously to previous figures, label (a) represents homogeneous models. We remind the reader that model (3) represents a minimally coupled quintessence model. At $z \approx 0$, all the models produce approximately the same number of haloes over a large mass range, however small differences take place at high masses.

At $z = 0.5$, we see that all models including the ΛCDM one are still giving approximately the same number of objects at low masses ($M \approx 10^{13}\,{\rm M}_\odot\,h^{-1}$), while at high masses ($M \approx 10^{15}\,{\rm M}_\odot\,h^{-1}$) the differences between the models (2), (3), (4) and the ΛCDM one become more pronounced. However, differences are negligible for model (1). Quantitatively speaking, at $z = 0.5$, model (4) with negative coupling constant $\xi = -0.087$ has roughly 22 per cent more haloes than the ΛCDM model. This value is roughly 11 per cent for model (2) and 17 per cent for the minimally coupled quintessence case with $\xi = 0$ (model 3). At higher redshifts, $z = 1$ and $z = 2$, we see that differences in the halo numbers appear also at low masses. At high redshifts, all the models here investigated predict a higher number of virialized haloes compared to the ΛCDM model. In particular, the number of objects in the non-minimally coupled case with negative coupling parameter $\xi = -0.087$ (model 4) is larger than what is predicted for a minimally coupled case (model 3). In the non-minimally coupled case with positive coupling constant $\xi = 0.088$ and $\xi = 0.123$ (models 1 and 2) instead, the number of objects is smaller. Fractional differences in the number of virialized haloes between different models and the ΛCDM model are presented in Table 2. Results are shown for three mass scales: $M > 10^{13}\,{\rm M}_\odot\,h^{-1}$, $M > 10^{14}\,{\rm M}_\odot\,h^{-1}$ and $M > 10^{15}\,{\rm M}_\odot\,h^{-1}$.

4.4 Abundance of haloes in clustering quintessence models

As shown in Section 4.2, the size and density of virialized haloes strongly depends on the background dynamics and change in the presence of the scalar field perturbations. Hence in clustering

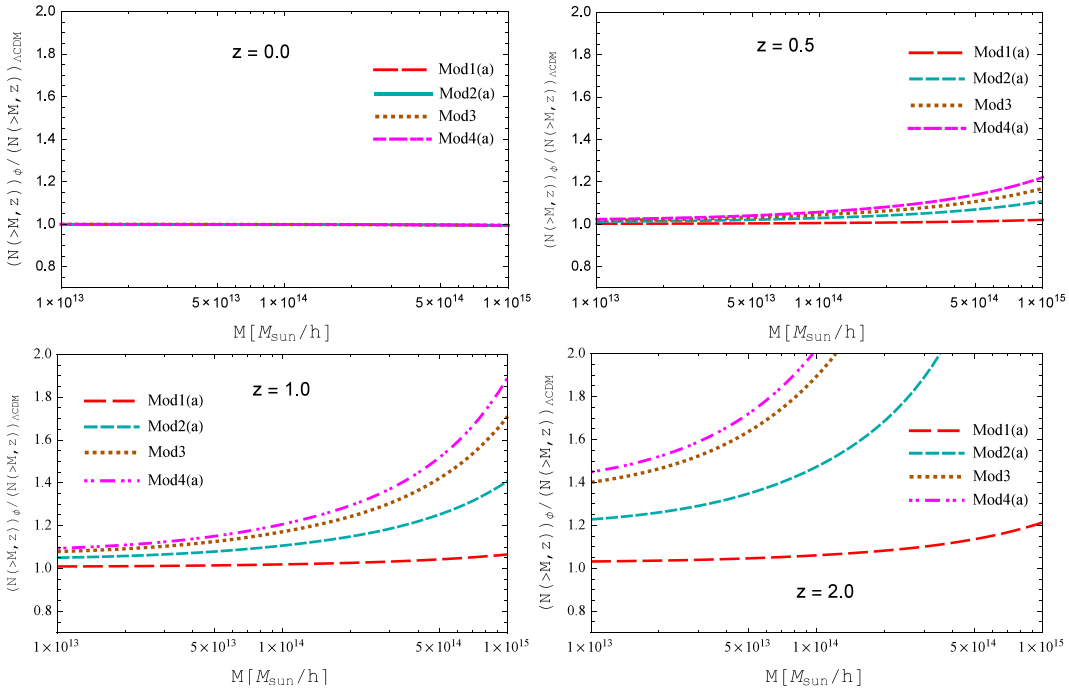

Figure 7. Ratio of the number of haloes above a given mass M at $z = 0$ (top left), $z = 0.5$ (top right), $z = 1.0$ (bottom left) and $z = 2.0$ (bottom right) between the minimally and the non-minimally coupled quintessence models and the concordance ΛCDM cosmology. Scalar field models have been assumed homogeneous. Line style and colours are as in Fig. 1.

Table 2. Numerical results for the fractional difference of number of haloes between homogeneous minimally and non-minimally coupled quintessence models and the concordance ΛCDM model. These results are presented at four different redshifts: $z = 0$, $z = 0.5$, $z = 1$ and $z = 2$ for objects with $M > 10^{13}\,\mathrm{M}_\odot\,h^{-1}$ (low-mass scale), $M > 10^{14}\,\mathrm{M}_\odot\,h^{-1}$ (intermediate mass scale) and $M > 10^{15}\,\mathrm{M}_\odot\,h^{-1}$ (high-mass end).

Model (1a)	$z = 0$	$z = 0.5$	$z = 1$	$z = 2$
$M > 10^{13}\,\mathrm{M}_\odot\,h^{-1}$	−0.1 per cent	0.3 per cent	0.9 per cent	3 per cent
$M > 10^{14}\,\mathrm{M}_\odot\,h^{-1}$	−0.2 per cent	0.6 per cent	2 per cent	6 per cent
$M > 10^{15}\,\mathrm{M}_\odot\,h^{-1}$	−0.6 per cent	2 per cent	7 per cent	21 per cent
Model (2a)	$z = 0$	$z = 0.5$	$z = 1$	$z = 2$
$M > 10^{13}\,\mathrm{M}_\odot\,h^{-1}$	−0.1 per cent	1.2 per cent	5 per cent	22 per cent
$M > 10^{14}\,\mathrm{M}_\odot\,h^{-1}$	−0.2 per cent	3 per cent	11 per cent	47 per cent
$M > 10^{15}\,\mathrm{M}_\odot\,h^{-1}$	−0.6 per cent	11 per cent	40 per cent	–
Model (3)	$z = 0$	$z = 0.5$	$z = 1$	$z = 2$
$M > 10^{13}\,\mathrm{M}_\odot\,h^{-1}$	−0.1 per cent	2 per cent	8 per cent	39 per cent
$M > 10^{14}\,\mathrm{M}_\odot\,h^{-1}$	−0.2 per cent	4 per cent	17 per cent	89 per cent
$M > 10^{15}\,\mathrm{M}_\odot\,h^{-1}$	−0.5 per cent	17 per cent	71 per cent	–
Model (4a)	$z = 0$	$z = 0.5$	$z = 1$	$z = 2$
$M > 10^{13}\,\mathrm{M}_\odot\,h^{-1}$	−0.1 per cent	2.3 per cent	9 per cent	43 per cent
$M > 10^{14}\,\mathrm{M}_\odot\,h^{-1}$	−0.2 per cent	6 per cent	21 per cent	101 per cent
$M > 10^{15}\,\mathrm{M}_\odot\,h^{-1}$	−0.5 per cent	22 per cent	89 per cent	–

models we should take into account the contribution of the scalar field density perturbations to the total mass of the haloes (see also Creminelli et al. 2010; Basse et al. 2011; Batista & Pace 2013; Pace et al. 2014b; Malekjani et al. 2015). We follow the formulation presented before in DE cosmologies where the total mass of the haloes is affected by DE perturbations (Batista & Pace 2013; Malekjani et al. 2015). The quantity $\epsilon(z) = M_{\rm DE}/M_{\rm m}$, representing the ratio of DE mass to matter mass, indicates how DE perturbations affect the total mass of virialized haloes. The mass of DE is defined according to the contribution of DE perturbation. If we assume the top-hat density profile and fully clustering DE, we have (see also Malekjani et al. 2015)

$$\epsilon(z) = \frac{\Omega_\phi(z)}{\Omega_{\rm m}(z)}\,\frac{\delta_{\rm de}(z)}{1+\delta_{\rm m}(z)}\,. \tag{29}$$

In Fig. 9, we show the redshift evolution of $\epsilon(z)$ on the basis of equation (29) for the different minimally and non-minimally coupled quintessence models considered in this work. We see that for all the non-minimally coupled models with positive or negative coupling constant ξ, the quantity ϵ is negative and for the minimally

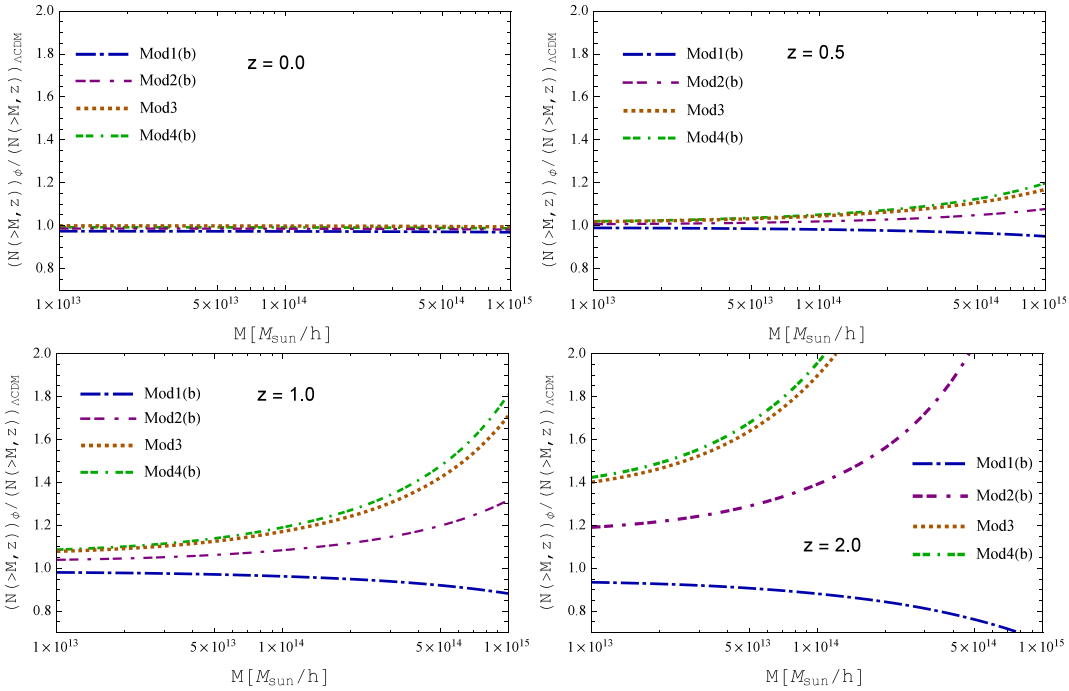

Figure 8. Ratio of the number of haloes above a given mass M at $z = 0$ (top left), $z = 0.5$ (top right), $z = 1.0$ (bottom left) and $z = 2.0$ (bottom right) between the minimally and the non-minimally coupled scalar field models considered in this work and the concordance ΛCDM cosmology. Here, we assume the clustering of scalar field models. Line style and colours are same as in Fig. 4.

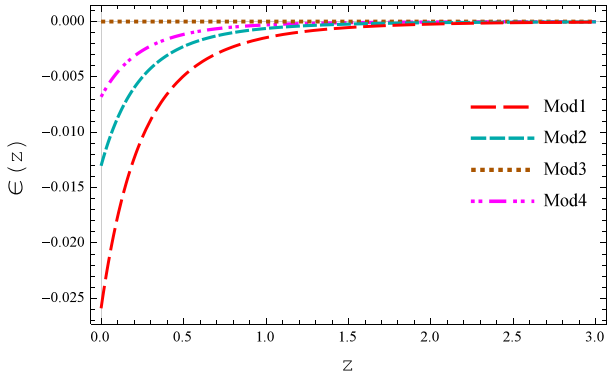

Figure 9. The redshift evolution of the ratio of DE mass to pressureless dark matter mass $\epsilon(z)$ calculated according to equation (29) for different scalar field models considered in this work. For the non-clustering minimally coupled scalar field case (model 3) we have $\epsilon = 0$ as expected. Line style and colours are as in Fig. 1.

coupled case (model 3) ϵ is zero. This result is expected, since δ_Φ for all non-minimally coupled models is negative and zero for model (3) (see also Fig. 4). We also see that for $z \gtrsim 1$, in all non-minimally coupled models ϵ approaches zero. This means that the contribution of the DE mass to the total mass of haloes is negligible at high redshifts. This is nothing else than requiring an EdS behaviour in the past. Moreover, models with larger coupling constant ξ give a higher contribution of the DE mass to the total mass of haloes. We notice that in these models the DE mass is negative and hence should be subtracted from the total mass of haloes.

Following Batista & Pace (2013), Pace et al. (2014b) and Malekjani et al. (2015), in the presence of DE mass contribution, the definition of the mass function in the Press–Schechter formalism is changed to

$$\frac{\mathrm{d}n(M, w, z)}{\mathrm{d}M} = \frac{\bar{\rho}_0}{M(1-\epsilon)} \frac{\mathrm{d}\nu(M, w, z)}{\mathrm{d}M} f(\nu)\,, \tag{30}$$

where $f(\nu)$ is given by equation (26). We notice that in clustering models, density perturbations of the scalar field change the function $f(\nu)$ via changing the quantities δ_c and σ. In Fig. 8, we show the predicted number of haloes calculated with the corrected mass function in equation (30) for clustering models divided by those obtained for the concordance ΛCDM model. In analogy to Fig. 7, we select four different redshifts $z = 0$, $z = 0.5$, $z = 1$ and $z = 2$. As in the previous section, clustering models are labelled with the letter '(b)'. Results for model (3) are similar to those obtained before and presented in Section 4.3. We see that at $z \approx 0$, all models roughly coincide with the ΛCDM case and differences are negligible. At $z = 0.5$ differences with the ΛCDM model are considerable at the high-mass tail ($M > 10^{15}\,\mathrm{M}_\odot\,h^{-1}$). In particular, we see that for model (4b) the number of haloes is roughly 20 per cent higher than that of the concordance ΛCDM model. This value is 17 per cent for model (3) and approximately 8 per cent for model (2b) and −5 per cent in the case of model (1b). The numerical values for the fractional difference of the number of haloes between the different clustering models considered in this work and the ΛCDM model are presented in Table 3. In analogy to Table (2), the results are reported for masses greater than 10^{13}, 10^{14} and $10^{15}\,\mathrm{M}_\odot\,h^{-1}$. At higher redshifts, $z = 1$ and $z = 2$, we see that the predicted number of haloes calculated for clustering models deviates from the ΛCDM expectation even at the low-mass end of the halo mass function. Generally, by comparing the results presented in Tables 2 and 3, we conclude that the number of virialized haloes estimated in clustering models is lower than that for homogeneous models. This result is due to the negative sign of δ_Φ and ϵ in clustering quintessence models. Differences between clustering and homogeneous models are more pronounced at the

Table 3. The fractional difference of number of haloes between clustering models in ST cosmologies and the concordance ΛCDM model. Results are shown at four different epochs: $z = 0$, $z = 0.5$, $z = 1$ and $z = 2$ for objects with $M > 10^{13}\,\mathrm{M}_\odot\,h^{-1}$, $M > 10^{14}\,\mathrm{M}_\odot\,h^{-1}$ and $M > 10^{15}\,\mathrm{M}_\odot\,h^{-1}$.

Model (1b)	$z = 0$	$z = 0.5$	$z = 1$	$z = 2$
$M > 10^{13}\,\mathrm{M}_\odot\,h^{-1}$	−2.6 per cent	−3.2 per cent	−4.5 per cent	−6.4 per cent
$M > 10^{14}\,\mathrm{M}_\odot\,h^{-1}$	−2.7 per cent	−3.6 per cent	−5.3 per cent	−12 per cent
$M > 10^{15}\,\mathrm{M}_\odot\,h^{-1}$	−3.1 per cent	−5 per cent	−11.8 per cent	−34 per cent
Model (2b)	$z = 0$	$z = 0.5$	$z = 1$	$z = 2$
$M > 10^{13}\,\mathrm{M}_\odot\,h^{-1}$	−1.4 per cent	0.6 per cent	3.8 per cent	19 per cent
$M > 10^{14}\,\mathrm{M}_\odot\,h^{-1}$	−1.5 per cent	1.9 per cent	8.5 per cent	39 per cent
$M > 10^{15}\,\mathrm{M}_\odot\,h^{-1}$	−1.9 per cent	7.7 per cent	32 per cent	–
Model (3)	$z = 0$	$z = 0.5$	$z = 1$	$z = 2$
$M > 10^{13}\,\mathrm{M}_\odot\,h^{-1}$	−0.1 per cent	2 per cent	8 per cent	39 per cent
$M > 10^{14}\,\mathrm{M}_\odot\,h^{-1}$	−0.2 per cent	4 per cent	17 per cent	89 per cent
$M > 10^{15}\,\mathrm{M}_\odot\,h^{-1}$	−0.5 per cent	17 per cent	71 per cent	–
Model (4b)	$z = 0$	$z = 0.5$	$z = 1$	$z = 2$
$M > 10^{13}\,\mathrm{M}_\odot\,h^{-1}$	−0.8 per cent	2 per cent	8.5 per cent	42 per cent
$M > 10^{14}\,\mathrm{M}_\odot\,h^{-1}$	−1 per cent	5 per cent	19 per cent	95 per cent
$M > 10^{15}\,\mathrm{M}_\odot\,h^{-1}$	−1.6 per cent	20 per cent	81 per cent	–

high-mass tail and at high redshifts, as expected. For example for model (1) where the coupling constant is the largest ($\xi = 0.123$), we see that at the high-mass tail ($M > 10^{15}\,\mathrm{M}_\odot\,h^{-1}$ at $z = 0$) the homogeneous model (1a) produces only 2.5 per cent more objects than in the clustering case (model 1b). This value is 7 per cent at $z = 0.5$, roughly 19 per cent at $z = 1$ and 55 per cent at $z = 2$. For other quintessence models we have similar results.

5 CONCLUSIONS

In the context of the SCM, we studied the non-linear growth of structures in ST cosmologies. In ST gravity, there is a non-minimally coupling between the scalar field and the Ricci scalar, the so-called non-minimally coupled quintessence models. We first studied the background expansion history in ST theories. We saw that in the case of positive non-minimally coupling parameter, $\xi > 0$ (model 1), the equation of state of the scalar field w_Φ can achieve the phantom regime ($w_\Phi < -1$) at high redshifts, while in the case of minimally coupled quintessence models (model 3), w_Φ remains always in the quintessence regime $-1 < w_\Phi < -1/3$, as expected (see the top panel of Fig. 2). The redshift evolution of the energy density Ω_Φ shows that all minimally and non-minimally coupled quintessence models considered in this work reduce to an EdS universe at high redshifts where the dynamics of the universe can be well described by the pressureless matter component (see middle panel of Fig. 2). All quintessence models in ST theories are characterized by $\Delta H(z) > 0$ at low redshift, meaning that all minimally and non-minimally coupled quintessence models have a larger Hubble parameter compared to the ΛCDM universe at low redshifts (see bottom panel of Fig. 2).

We then followed the evolution of matter perturbations within the ST gravity on sub-Hubble scales. In particular, we focused on the scalar field perturbations due to the non-minimal coupling between the scalar field and the Ricci scalar, the so-called clustering non-minimally coupled quintessence models. When we ignore the scalar field perturbations and assume that the scalar field is important only at the background level, the model is the so-called homogeneous non-minimally coupled quintessence model. The equation describing the evolution of matter overdensities in ST theories is similar to the one found in general relativistic models, albeit in this case the Newtonian gravitational constant G_N is replaced by the effective gravitational constant G_eff (equation 20). Since there is a difference between the definition of G_eff in homogeneous (equation 22) and clustering (equation 20) non-minimally coupled quintessence models, we infer that the evolution of matter perturbations on the basis of equation (19) differs between clustering and homogeneous non-minimally coupled quintessence models. We saw that for higher values of the coupling parameter ξ, the effective gravitational constant $G_\mathrm{eff}^{(p)}$ defined in clustering non-minimally quintessence model is higher than the same quantity $G_\mathrm{eff}^{(h)}$ defined in homogeneous non-minimally coupled quintessence models (Fig. 3). Hence we conclude that the scalar field perturbations directly affect the effective gravitational constant in ST cosmologies. In the case of minimally coupled quintessence models ($\xi = 0$) since the perturbations of scalar field are vanishing, the difference between these two different definitions of effective gravitational constant is zero. The linear growth factor depends strongly on the sign of the coupling parameter ξ, so that the growth factor for non-minimally coupled quintessence with negative (positive) coupling ξ is larger (smaller) than in minimally coupled quintessence (top panel of Fig. 4).

We showed that independently of the sign of the coupling parameter, the perturbations of the scalar field are always negative (bottom panel of Fig. 4), so that the clustering non-minimally quintessence models can reproduce the void DE structures. Due to the negative sign of the scalar field perturbations, the linear growth factor in clustering quintessence models is smaller than that obtained in homogeneous quintessence models (top panel of Fig. 4).

As next step we calculated the SCM parameters δ_c and Δ_vir in the context of homogeneous and clustering non-minimally coupled quintessence models. Due to the negative sign of the scalar field perturbations, we notice that the linear overdensity δ_c is smaller with respect to the case when the scalar field is homogeneous (see Fig. 5). The redshift evolution of the virial overdensity Δ_vir parameter shows that in both homogeneous and clustering quintessence models the scalar field sector slows down the collapse and the formation of overdense regions as it happens for DE models in standard GR gravity (see Fig. 6).

With this point of the discussion, we want to stress the point that the results here obtained for both the linear growth factor ($D(a)$)

and linear overdensity parameter (δ_c) are more general than those in Pace et al. (2014a), where the effective gravitational constant was approximated to $G_{\rm eff} \simeq G_{\rm N}/F$ for a direct comparison with N-body simulations.

We finally investigated the number count of haloes for non-minimally coupled quintessence models taking into account the scalar field perturbations. In the case of homogeneous models, we showed that all the models here investigated give an excess of structures with respect to the concordance ΛCDM model. The differences between non-minimally coupled models and the ΛCDM model are more pronounced for high masses and high redshifts. We also notice that the number of haloes in non-minimally coupled quintessence models with negative (positive) coupling parameter ξ is higher (lower) than that obtained in the minimally coupled quintessence case (see Fig. 7).

When the scalar field is clustering, we should in principle modify the mass of the halo. When doing this, we obtain similar results to the homogeneous case, except for model (1). In model (1), we see that the number of haloes is lower than in the reference ΛCDM universe. Since scalar field perturbations are negative (see Fig. 9), the predicted number of haloes is smaller compared to the homogeneous models (see Tables 2 and 3).

ACKNOWLEDGEMENTS

Work of M. Malekjani and N. Nazari-Pooya has been supported by Iran Science Elites Federation.

REFERENCES

Abramo L. R., Batista R. C., Liberato L., Rosenfeld R., 2007, J. Cosmol. Astropart. Phys., 11, 12
Abramo L. R., Batista R. C., Liberato L., Rosenfeld R., 2008, Phys. Rev. D, 77, 067301
Abramo L. R., Batista R. C., Rosenfeld R., 2009, J. Cosmol. Astropart. Phys., 7, 40
Acquaviva V., Baccigalupi C., Perrotta F., 2004, Phys. Rev. D, 70, 023515
Allen S. W., Schmidt R. W., Ebeling H., Fabian A. C., van Speybroeck L., 2004, MNRAS, 353, 457
Amendola L., Kunz M., Sapone D., 2008, J. Cosmol. Astropart. Phys., 4, 13
Ascasibar Y., Yepes G., Gottlöber S., Müller V., 2004, MNRAS, 352, 1109
Avila-Reese V., Firmani C., Hernández X., 1998, ApJ, 505, 37
Barkana R., Loeb A., 2001, Phys. Rep., 349, 125
Basilakos S., 2009, MNRAS, 395, 2347
Basilakos S., Perivolaropoulos L., 2008, MNRAS, 391, 411
Basse T., Eggers Bjælde O., Wong Y. Y. Y., 2011, J. Cosmol. Astropart. Phys., 10, 38
Batista R. C., Pace F., 2013, J. Cosmol. Astropart. Phys., 6, 44
Benjamin J. et al., 2007, MNRAS, 381, 702
Bergmann P. G., 1968, Int. J. Theor. Phys., 1, 25
Bertotti B., Iess L., Tortora P., 2003, Nature, 425, 374
Bertschinger E., 1985, ApJS, 58, 39
Boisseau B., Esposito-Farèse G., Polarski D., Starobinsky A. A., 2000, Phys. Rev. Lett., 85, 2236
Bond J. R., Cole S., Efstathiou G., Kaiser N., 1991, ApJ, 379, 440
Brans C., Dicke R. H., 1961, Phys. Rev., 124, 925
Bromm V., Yoshida N., 2011, ARA&A, 49, 373
Bueno Sanchez J. C., Perivolaropoulos L., 2010, Phys. Rev. D, 81, 103505
Caresia P., Matarrese S., Moscardini L., 2004, ApJ, 605, 21
Carroll S. M., 2001, Living Rev. Relativ., 4, 1
Chiba T., 1999, Phys. Rev. D, 60, 083508
Ciardi B., Ferrara A., 2005, Space Sci. Rev., 116, 625
Copeland E. J., Sami M., Tsujikawa S., 2006, Int. J. Mod. Phys. D, 15, 1753
Creminelli P., D'Amico G., Noreña J., Senatore L., Vernizzi F., 2010, J. Cosmol. Astropart. Phys., 3, 27
de Putter R., Huterer D., Linder E. V., 2010, Phys. Rev. D, 81, 103513
Dutta S., Maor I., 2007, Phys. Rev. D, 75, 063507
Esposito-Farèse G., Polarski D., 2001, Phys. Rev. D, 63, 063504
Fan Y., Wu P., Yu H., 2015, Phys. Rev. D, 92, 083529
Ferreira P. G., Joyce M., 1997, Phys. Rev. Lett., 79, 4740
Ferreira P. G., Joyce M., 1998, Phys. Rev. D, 58, 023503
Fillmore J. A., Goldreich P., 1984, ApJ, 281, 1
Fu L. et al., 2008, A&A, 479, 9
Gannouji R., Polarski D., Ranquet A., Starobinsky A. A., 2006, J. Cosmol. Astropart. Phys., 9, 16
Gunn J. E., Gott J. R., III, 1972, ApJ, 176, 1
Guth A. H., 1981, Phys. Rev. D, 23, 347
Hawkins E. et al., 2003, MNRAS, 346, 78
Hoffman Y., Shaham J., 1985, ApJ, 297, 16
Horellou C., Berge J., 2005, MNRAS, 360, 1393
Hwang J.-C., Noh H., 2005, Phys. Rev. D, 71, 063536
Jassal H. K., 2009, Phys. Rev. D, 79, 127301
Jassal H. K., 2010, Phys. Rev. D, 81, 083513
Jassal H. K., 2012, Phys. Rev. D, 86, 043528
Komatsu E. et al., 2009, ApJS, 180, 330
Kowalski M. et al., 2008, ApJ, 686, 749
Krauss L. M., Chaboyer B., 2003, Science, 299, 65
Lahav O., Lilje P. B., Primack J. R., Rees M. J., 1991, MNRAS, 251, 128
Li M., Li X.-D., Wang S., Zhang X., 2009, J. Cosmol. Astropart. Phys., 6, 36
Li J.-X., Wu F.-Q., Li Y.-C., Gong Y., Chen X.-L., 2015, Res. Astron. Astrophys., 15, 2151
Linde A., 1990, Phys. Lett. B, 238, 160
Mainini R., 2009, J. Cosmol. Astropart. Phys., 4, 17
Malekjani M., Naderi T., Pace F., 2015, MNRAS, 453, 4148
Mantz A., Allen S. W., Ebeling H., Rapetti D., 2008, MNRAS, 387, 1179
Maor I., Lahav O., 2005, J. Cosmol. Astropart. Phys., 7, 3
McDonald P. et al., 2005, ApJ, 635, 761
Mota D. F., van de Bruck C., 2004, A&A, 421, 71
Naderi T., Malekjani M., Pace F., 2015, MNRAS, 447, 1873
Nesseris S., Perivolaropoulos L., 2008, Phys. Rev. D, 77, 023504
Nordtvedt Jr, K., 1970, ApJ, 161, 1059
Pace F., Waizmann J.-C., Bartelmann M., 2010, MNRAS, 406, 1865
Pace F., Fedeli C., Moscardini L., Bartelmann M., 2012, MNRAS, 422, 1186
Pace F., Moscardini L., Crittenden R., Bartelmann M., Pettorino V., 2014a, MNRAS, 437, 547
Pace F., Batista R. C., Del Popolo A., 2014b, MNRAS, 445, 648
Padmanabhan T., 2003, Phys. Rep., 380, 235
Peacock J. A., 1999, Cosmological Physics. Cambridge Univ. Press, Cambridge
Peebles P. J. E., 1993, Principles of Physical Cosmology. Princeton Univ. Press, Princeton, NJ
Peebles P. J., Ratra B., 2003, Rev. Mod. Phys., 75, 559
Percival W. J. et al., 2010, MNRAS, 401, 2148
Perlmutter S. et al., 1999, ApJ, 517, 565
Perrotta F., Baccigalupi C., 2002, Phys. Rev. D, 65, 123505
Perrotta F., Baccigalupi C., Matarrese S., 2000, Phys. Rev. D, 61, 023507
Pettorino V., Baccigalupi C., 2008, Phys. Rev. D, 77, 103003
Planck Collaboration XIII, 2015, preprint (arXiv:1502.01589)
Polarski D., Gannouji R., 2008, Phys. Lett. B, 660, 439
Press W. H., Schechter P., 1974, ApJ, 187, 425
Ratra B., Peebles P. J. E., 1988, Phys. Rev. D, 37, 3406
Reasenberg R. D. et al., 1979, ApJ, 234, L219
Riazuelo A., Uzan J.-P., 2002, Phys. Rev. D, 66, 023525
Riess A. G. et al., 1998, AJ, 116, 1009
Ryden B. S., Gunn J. E., 1987, ApJ, 318, 15
Sahni V., Starobinsky A., 2000, Int. J. Mod. Phys. D, 9, 373
Sheth R. K., Tormen G., 1999, MNRAS, 308, 119
Sheth R. K., Tormen G., 2002, MNRAS, 329, 61
Starobinsky A. A., 1980, Phys. Lett. B, 91, 99
Subramanian K., Cen R., Ostriker J. P., 2000, ApJ, 538, 528
Unnikrishnan S., Jassal H. K., Seshadri T. R., 2008, Phys. Rev. D, 78, 123504
Uzan J.-P., 1999, Phys. Rev. D, 59, 123510

Villata M., 2012, Ap&SS, 339, 7
Wagoner R. V., 1970, Phys. Rev. D, 1, 3209
Wang L., Steinhardt P. J., 1998, ApJ, 508, 483
Wang Y., Tegmark M., 2005, Phys. Rev. D, 71, 103513
Weinberg S., 1989, Rev. Mod. Phys., 61, 1
Weller J., Lewis A. M., 2003, MNRAS, 346, 987
Wetterich C., 1988, Nucl. Phys. B, 302, 668
White S. D. M., Rees M. J., 1978, MNRAS, 183, 341
Williams L. L. R., Babul A., Dalcanton J. J., 2004, ApJ, 604, 18
Wintergerst N., Pettorino V., Mota D. F., Wetterich C., 2010, Phys. Rev. D, 81, 063525

APPENDIX A: USEFUL EQUATIONS IN TERMS OF THE PLANCK MASS

Since different works in literature use different definitions of the function F characterizing the coupling between the scalar field and the Ricci scalar, for the sake of completeness, here we write the most important equations used in this work relaxing the common notation $8\pi G = 1$. This will help the reader to implement the following equations correctly from a dimensional point of view. We also remind the reader that, expressing physical quantities in units of mass ($[M]$), the density and the scalar field potential have units of $[M^4]$, the Hubble function and time derivatives have units of $[M]$ and finally the scalar field is expressed in units of the reduced Planck mass ($M_{\rm pl}^2 = 1/(8\pi G)$), where we have set $\hbar$ (Planck constant) and c (speed of light) to unity. The function F and the coupling constant ξ are assumed to be dimensionless quantities.

The function $F(\Phi)$ is therefore

$$F(\phi) = 1 + \xi \left[\left(\frac{\Phi}{M_{\rm pl}} \right)^2 - \left(\frac{\Phi_0}{M_{\rm pl}} \right)^2 \right] , \tag{A1}$$

and the density and the pressure of the scalar field are

$$\rho_\Phi = \frac{1}{2}\dot{\Phi}^2 + U(\Phi) - 3H M_{\rm pl}^2 \dot{F} , \tag{A2}$$

$$p_\Phi = \frac{1}{2}\dot{\Phi}^2 - U(\Phi) + M_{\rm pl}^2(\ddot{F} + 2H\dot{F}) . \tag{A3}$$

Hence Friedmann equations read

$$3F(\Phi)H^2 = 8\pi G \left(\rho_{\rm m} + \frac{1}{2}\dot{\Phi}^2 + U \right) - 3H\dot{F} , \tag{A4}$$

$$-2F(\Phi)\dot{H} = 8\pi G \left(\rho_{\rm m} + \dot{\Phi}^2 \right) + \ddot{F} - H\dot{F} , \tag{A5}$$

$$\frac{\ddot{a}}{a} = -\frac{4\pi G}{3F} \left[\rho_{\rm m} + 2\dot{\Phi}^2 - 2U + 3M_{\rm pl}^2(\ddot{F} + H\dot{F}) \right] . \tag{A6}$$

Note that equation (A6) corrects a typo in equation (22) of Pace et al. (2014a).

The Klein–Gordon equation can be written in a more general form by noticing that $R = 6(2H^2 + \dot{H})$:

$$\ddot{\Phi} + 3H\dot{\Phi} + \frac{{\rm d}U}{{\rm d}\Phi} = \frac{1}{2}M_{\rm pl}^2 \frac{{\rm d}F}{{\rm d}\Phi} R . \tag{A7}$$

The two different forms of the effective gravitational constant read

$$G_{\rm eff}^{(h)} = \frac{G_{\rm N}}{F} \left(\frac{2F + 2M_{\rm pl}^2 F_{,\Phi}^2}{2F + 3M_{\rm pl}^2 F_{,\Phi}^2} \right) = \frac{G_{\rm N}}{F} \frac{2 + 2\omega_{\rm JDB}^{-1}}{2 + 3\omega_{\rm JDB}^{-1}} , \tag{A8}$$

$$G_{\rm eff}^{(p)} = \frac{G_{\rm N}}{F} \left(\frac{2F + 4M_{\rm pl}^2 F_{,\Phi}^2}{2F + 3M_{\rm pl}^2 F_{,\Phi}^2} \right) = \frac{G_{\rm N}}{F} \frac{2 + 4\omega_{\rm JDB}^{-1}}{2 + 3\omega_{\rm JDB}^{-1}} , \tag{A9}$$

where we introduced the *Jordan–Brans–Dicke* parameter $\omega_{\rm JDB}$:

$$\omega_{\rm JDB}^{-1} = M_{\rm pl}^2 F_{,\Phi}^2 / F . \tag{A10}$$

By using equation (A10), we see that GR is recovered for $\omega_{\rm JDB} \gg 1$. In addition, we also notice that for $\omega_{\rm JDB} \gg 1$ we obtain $G_{\rm eff}^{(h)} = G_{\rm eff}^{(p)} \simeq G_{\rm N}/F$. This shows once again, from a different point of view, that in the general relativistic regime, fluctuations of the scalar field become unimportant.

This paper has been typeset from a TEX/LATEX file prepared by the author.